JOURNAL OF AIRCRAFT
Vol. 42, No. 2, March–April 2005

# Aerodynamic and Static Aeroelastic Characteristics of a Variable-Span Morphing Wing

Jae-Sung Bae,* T. Michael Seigler,† and Daniel J. Inman‡
*Virginia Polytechnic Institute and State University, Blacksburg, Virginia 24061*

**The morphing concept for unmanned aerial vehicles is a topic of current research interest in aerospace engineering. One concept of morphing is to change the wing configuration during flight to allow for multiple flight regimes. A particular approach to planform morphing is a variable-span morphing wing to increase wingspan to reduce induced drag and increase range and endurance. The wing area and the aspect ratio of the variable-span morphing wing increase as the wingspan increases. This means that the total lift increases while the induced drag is reduced, whereas the wing-root bending moment increases, thus, requiring a larger bending stiffness of the wing structure. Therefore, a study of the variable-span morphing wing requires not only aerodynamic analysis but also an investigation of the aeroelastic characteristics of the wing. The aerodynamic characteristics of the variable-span morphing wing are investigated, and a static aeroelastic analysis is performed.**

## Nomenclature

| | | |
|---|---|---|
| $b$ | = | wing span of conventional wing |
| $C_D$ | = | total drag coefficient |
| $C_{Di}$ | = | induced drag coefficient |
| $C_{D0}$ | = | profile drag coefficient |
| $C_L$ | = | lift coefficient |
| $C_M$ | = | moment coefficient |
| $D$ | = | drag |
| $f_0$ | = | aerodynamic force due to airfoil shape and angle of attack |
| $[GK]$ | = | generalized stiffness matrix |
| $[K]$ | = | stiffness matrix |
| $L$ | = | lift |
| $M$ | = | moment |
| $[M]$ | = | mass matrix |
| $[\bar{Q}]$ | = | aerodynamic influence coefficient |
| $q$ | = | dynamic pressure |
| $S$ | = | wing area of morphing wing |
| $S_C$ | = | wing area of conventional wing |
| $\bar{S}$ | = | area ratio, $S/S_C$ |
| $V$ | = | speed |
| $x$ | = | wing displacement |
| $y_e$ | = | wing extension |
| $\eta$ | = | modal coordinate |
| $\rho$ | = | air density |

## Introduction

MORPHING concepts for aerial vehicles, particularly unmanned aerial vehicles, have been a significant topic in recent aerospace research. The morphing wing is a birdlike wing that has the ability to adapt to accommodate multiple flight regimes or to obtain better flight performance.[1] A number of studies investigating morphing concepts have been performed over the past decade.

Methods of wing morphing include camber change,[2,3] wing twist,[4] wing sweep change, and wing span change.[5] In camber change, the adaptive airfoil can change camber to obtain a desired lift, thus, eliminating the need for conventional control surfaces. In morphing via variable twist, the wing is configured to optimize the twist angle to obtain low-drag and high-lift aerodynamic characteristics. The wing sweep change and the wing span change are designed to change the wing configuration of an aerial vehicle for various flight conditions. Variable wing sweep has been successfully applied in various modern U.S. military aircraft such as the F-14, F-111, and B-1 (Ref. 3). These aircraft change their wing sweep angle to decrease drag as the speed increases.

Recently, Gern et al.[2] performed a structural and aeroelastic analysis of an unmanned combat aerial vehicle with morphing airfoils. Sanders et al.[3] investigated the aerodynamic and aeroelastic characteristics of a morphing wing with a conformal control surface. Blondeau et al.[5] developed an inflatable telescopic spar and performed wind-tunnel test of a variable-span wing with this spar.

A variable-span morphing wing, as shown in Fig. 1, is designed to change its wing span for various flight conditions to reduce drag. As a result of increasing the wing span, the aspect ratio and wing area increase and the spanwise lift distribution decreases for the same lift. Thus, the drag of the morphing wing decreases, and consequently, the range of the aerial vehicle is increased. Unfortunately, the wing-root bending moment (WRBM) can be increased considerably due to the increase of the wing span. Therefore, not only the aerodynamic characteristics but also aeroelastic characteristics should be investigated in the design of the variable-span morphing wing.

The purpose of the present study is to investigate the aerodynamic and aeroelastic characteristics of a variable-span morphing wing applied to a long-range cruise missile in an effort to increase range. The panel code[6] used in this study is a subsonic doublet-hybrid method (DHM) for the computation of subsonic aerodynamic forces. MSC/NASTRAN is used to model the wing-box structure of the variable-span morphing wing. Effects of the wing span changes on the aerodynamic characteristics and the spanwise load distributions of the morphing wing are investigated. Advantages of wing span change, such as increased range, are also considered. Furthermore, aerodynamic deformations of the morphing wing are calculated, and its aeroelastic characteristics are investigated.

## Analytical Methods

### Variable-Span Wing Configuration

In Fig. 1 the concept of variable-span morphing for a long-range cruise missile is demonstrated by showing the original wing, with no extension, and the fully extend wing: In this case, full extension

Received 05 August 2003; revision received 25 March 2004; accepted for publication 9 April 2004. 

*Postdoctoral Research Associate, Center for Intelligent Material Systems and Structures, Department of Mechanical Engineering; currently Ph.D., Senior Researcher, Wind Power/Fluid Machinery Research Center, Korea Institute of Energy Research, 71-2 Jang-dong, Yuseong-gu, Daejon, 305-343, Korea; Jsbae@kier.re.kr; jsbae@vt.edu. Member AIAA.

†Graduate Research Assistant, Center for Intelligent Material Systems and Structures, Department of Mechanical Engineering; tseigler@vt.edu.

‡G. R. Goodson Professor and Director, Center for Intelligent Material Systems and Structures, Department of Mechanical Engineering; dinman@vt.edu. AIAA Fellow.

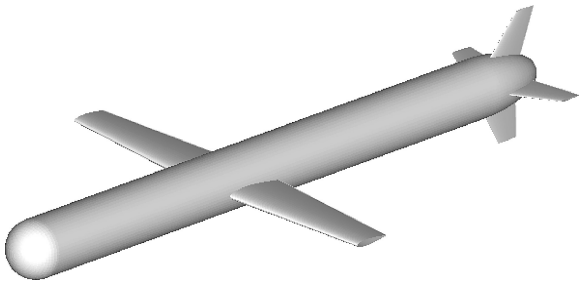

**a) Original wing**

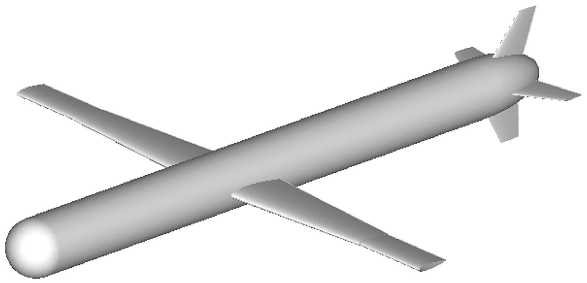

**b) 50% Span-extended wing**

**Fig. 1 Cruise missile with VSMW.**

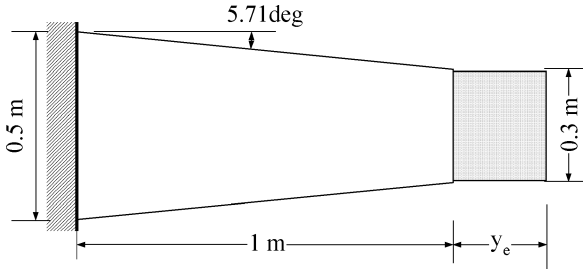


**Fig. 2 Configuration of VSMW.**

represents a 50% increase in wing span relative to the original configuration. Figure 2 shows a detailed configuration of the morphing wing used in subsequent analyses. The root-chord length is 0.51 m, the wing span of the original wing is 1.0 m, and the taper ratio is 0.6. The wing area of the original, or conventional, wing is 0.413 $m^2$ with an aspect ratio of 5.0. The Mach number upper limit of a cruise missile is approximately 0.7 and the wing load is in the range of thousands of kilograms per square meters (hundreds of pounds per square foot). Figure 3 shows the changes in aspect ratio and wing area ratio of the variable-span morphing wing as the wing span increases. The wing ratio is the ratio of the extended wing area divided by the original wing area. The solid line with a hollow circle is the aspect ratio change and the dashed line with a solid square in Fig. 3 is the wing area change. When fully extended to 50%, the aspect ratio is 8.18 and the wing area is 0.568 $m^2$. (The area ratio is 1.38.)

### Aerodynamic and Structural Models

Figure 4 shows the aerodynamic and structural models of the variable-span morphing wing. The aerodynamic mesh of the conventional wing for the DHM code[6] is 10 × 20. DHM is used to calculate the relationship between the pressure difference at the doublet point and the downwash at the receiving point using the kernel function.[7,8] When the morphing wing is fully extended, the aerodynamic mesh is 10 × 30. The structural model used in the present study is a wing-box model.[9] The structure of the variable-span morphing wing is composed of two wings: One is a main wing box and the other is a moving wing box, which extends from the main wing. Each wing box is composed of spar cabs, sparwebs, and skins. MSC/NASTRAN is used for constructing the wing-box models. Table 1 shows the structural properties of the elements used in the building of the morphing wing. Figure 5 shows the coupled finite element (FE) models of the morphing wing with 0, 30, and 50% span extensions. The main wing and the moving wing are composed of four wing-box sections and two wing-box sections, respectively. In these FE models, the moving wing box is constrained to the main wing box by using the multipoint constraint elements of MSC/NASTRAN. The structural characteristics of the variable-span morphing wing (VSMW) are significantly dependent on the boundary conditions at the joint, and the wing will contain some nonlinearities such as freeplay. These problems should be explored but are not investigated in the present study.

**Table 1 Element properties of morphing wing**

| Structural element | Unit | Value |
|---|---|---|
| *Main wing* | | |
| Sparweb (shear panel) | Thickness, mm | 2.5 |
| Rib (shear panel) | Thickness, mm | N/A |
| Skin (membrane) | Thickness, mm | 1.0 |
| Sparcab (rod) | Area, $mm^2$ | 32. |
| Mass | Mass, kg | 0.9 |
| *Moving wing* | | |
| Sparweb (shear panel) | Thickness, mm | 0.1 |
| Rib (shear panel) | Thickness, mm | N/A |
| Skin (membrane) | Thickness, mm | 0.04 |
| Sparcab (rod) | Area, $mm^2$ | 0.03 |
| Mass | Mass, kg | 0.59 |

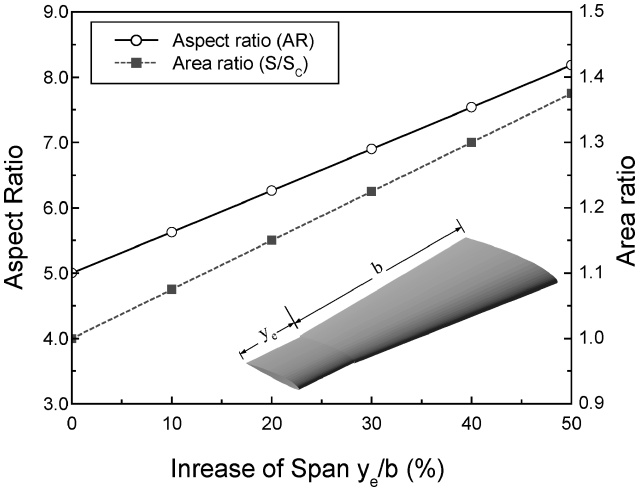


**Fig. 3 Changes of aspect ratio and wing area.**

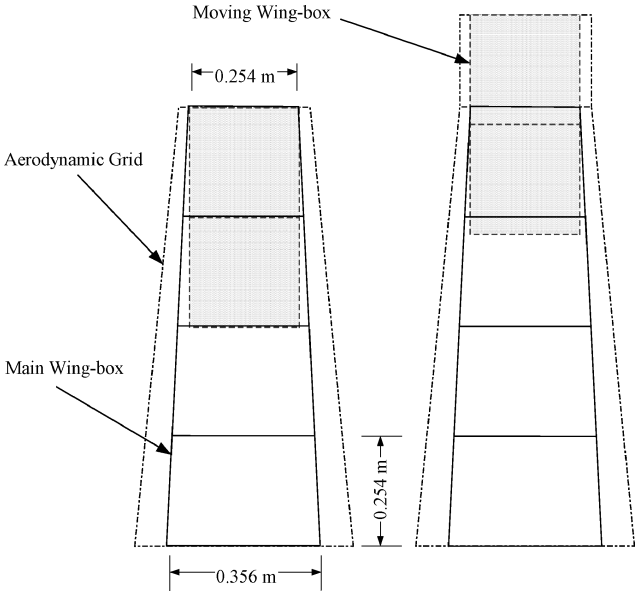


**Fig. 4 Aerodynamic and structural models.**

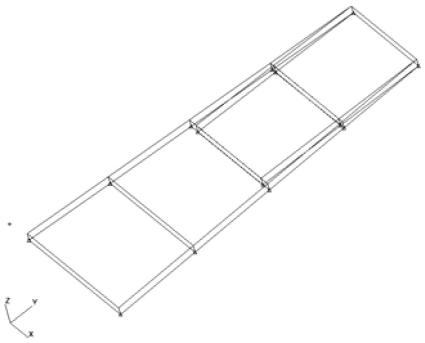

**a) 0% Span extended**

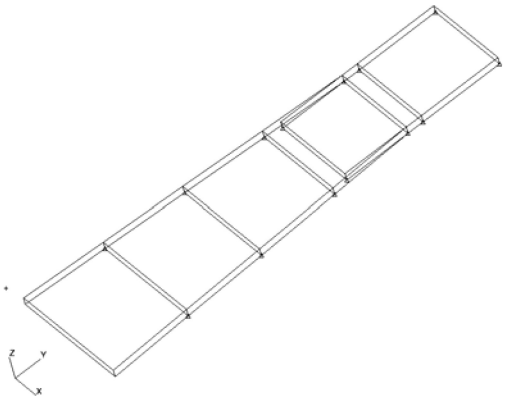

**b) 30% Span extended**

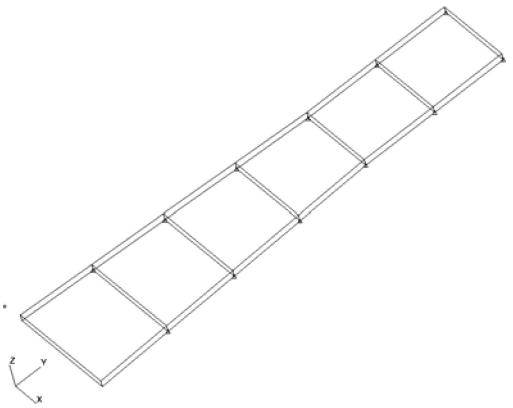

**c) 50% Span extended**

**Fig. 5 FE models of VSMW with various span lengths.**

#### Aerodynamic Coefficients

The wing area and aspect ratio of a conventional wing is fixed. To increase the lift, the lift coefficient should be increased. This is typically accomplished via an increase in the angle of attack. Alternatively, a VSMW can change its lift coefficient, wing area, and aspect ratio by changing its wing span. Hence, we should compare the lifts of the conventional wing and the morphing wing instead of the lift coefficient $C_L$, which requires a new definition for the aerodynamic coefficient. The definitions of the aerodynamic coefficients used in the present study are

$$C_L\bar{S} = L/qS_C, \qquad C_M\bar{S} = M/qS_CC, \qquad C_D\bar{S} = D/qS_C \quad (1)$$

where, $\bar{S}(=S/S_C)$, $S_C$, and $q(=\rho V^2/2)$ are the area ratio, the area of the conventional wing, and the dynamic pressure, respectively.

#### Aeroelastic Equations

The aeroelastic equations for the wing structure can be written as

$$[M]\{\ddot{x}\} + [K]\{x\} = \{f\} \quad (2)$$

where $\{f\}$ and $\{x\}$ are the aerodynamic force vector and structural displacement vector, respectively.

For the static problem, such as divergence or aerodynamic deformation, Eq. (2) can be written as

$$[K]\{x\} = \{f\} \quad (3)$$

In Eq. (3), the aerodynamic force vector can be written as

$$\{f\} = \{f(x)\} + \{f_0\} \quad (4)$$

where the first term, $\{f(x)\}$, is due to the wing deflection and the last term, $\{f_0\}$, is due to the airfoil shape or the angle of attack.

When the modal approach is used, Eq. (3) can be transformed to the generalized coordinates of Eq. (2) as

$$[GK]\{\eta\} = [\phi]^T\{f(x)\} + [\phi]^T\{f_0\} \quad (5)$$

where $\{\eta\}$, and $[\phi]$ are the displacement vector and the modal matrix, respectively. These quantities are defined as

$$\{x\} = [\phi]\{\eta\} \quad (6)$$

$$[GK] = [\phi]^T[K][\phi] = \left[\omega_i^2\right] \quad (7)$$

where $[GK]$ and $[\phi]$ can be obtained from the free-vibration analysis of Eq. (2).

The generalized aerodynamic influence coefficients (AIC) $[\bar{Q}]$ are introduced as follows:

$$[\phi]^T\{f(x)\} = q[\phi]^T[Q][\phi]\{\eta\} = q[\bar{Q}]\{\eta\} \quad (8)$$

Finally, the generalized static aeroelastic equations can be written as

$$[GK]\{\eta\} = q[\bar{Q}]\{\eta\} + [\phi]^T\{f_0\} \quad (9)$$

For a given dynamic pressure, Eq. (9) can be solved iteratively to obtain the modal displacement $\{\eta\}$. Also, Eq. (9) can be solved directly if $([GK] - q[\bar{Q}])$ is not singular, and the wing displacement can be easily obtained from Eq. (6).

Divergence is a static aeroelastic instability, and the divergence equations can be obtained from Eq. (9). When the last term on the right-hand side of Eq. (9) is ignored, the divergence equations can be written as

$$\lambda_D\{\eta\} = [GK]^{-1}[\bar{Q}]\{\eta\} \quad (10)$$

where

$$\lambda_D = 1/q_D \quad (11)$$

The $\lambda_{Di}(i = 1 \sim n)$ can be obtained by solving the eigenvalue problem of Eq. (11). When the largest positive value of the real eigenvalues is taken, divergence speed $V_D$ can be calculated by

$$V_D = \sqrt{2/\rho\lambda_D} \quad (12)$$

## Aerodynamic Characteristics

#### Aerodynamics

Figure 6 shows the lift coefficient contours of a VSMW for changes in wing span and angle of attack. The contours of Fig. 6 are similar to a flat surface, which means that the lift coefficient $C_L\bar{S}$ is linearly proportional to both the angle of attack and wing span. For the same wing span and angle of attack, the lift coefficient at $M = 0.7$ is larger than that of $M = 0.0$. Figure 7 shows the angle of attack required to produce the desired lift. As shown in Fig. 7, the lift coefficient is linearly proportional to the angle of attack, (AOA). Hence, to obtain the same lift, the conventional wing requires a larger AOA than the variable-span morphing wing.

Figure 8 shows the lift coefficient contours for changes of the wing span and Mach number when the AOA is 1.0 deg. The contours represent a curved surface, and the increment of the lift coefficient

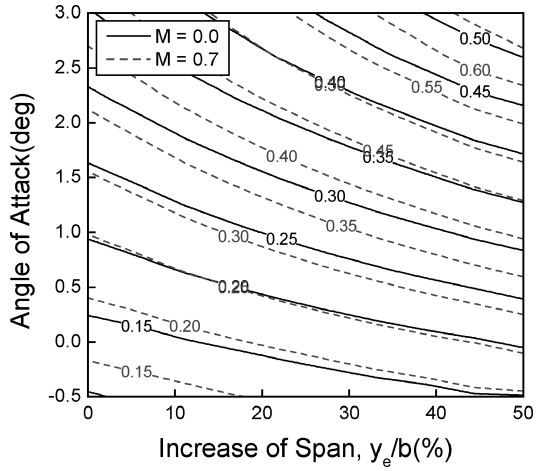


**Fig. 6 Lift coefficient contour for AOA and increase of wing span.**

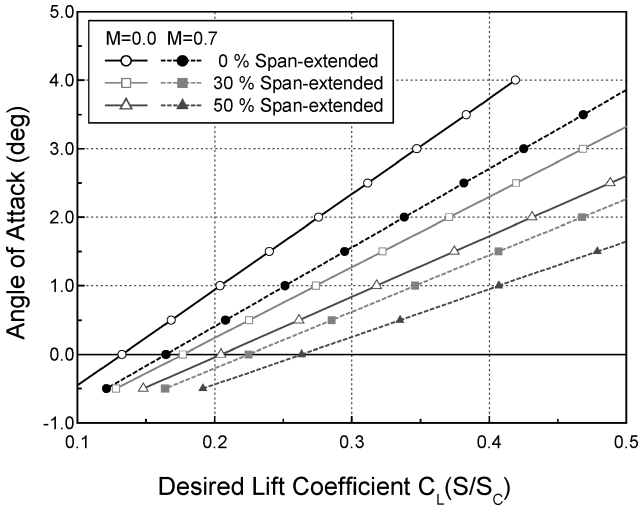


**Fig. 7 Desired lift vs angle of attack.**

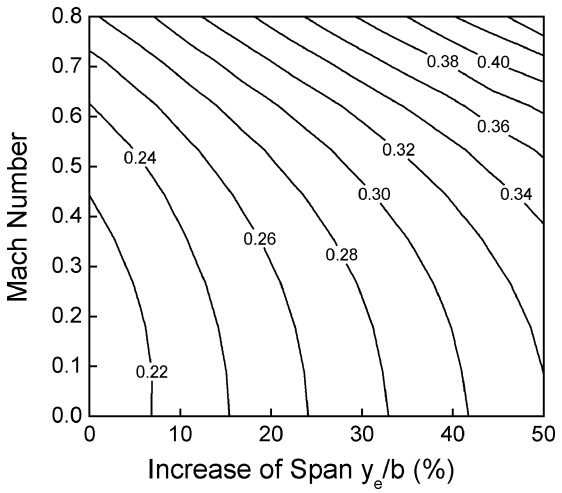


**Fig. 8 Lift coefficient contour for Mach number and increase of wing span, AOA = 1.0 deg.**

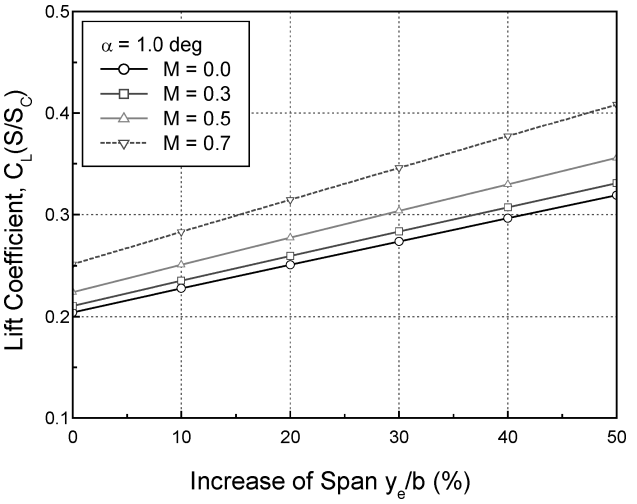


**Fig. 9 Increase of span vs lift coefficient, AOA = 1.0 deg.**

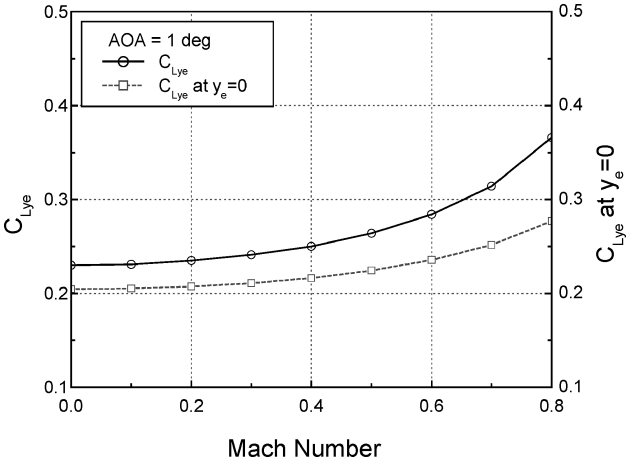


**Fig. 10 Mach number vs lift coefficient derivative, AOA = 1.0 deg.**

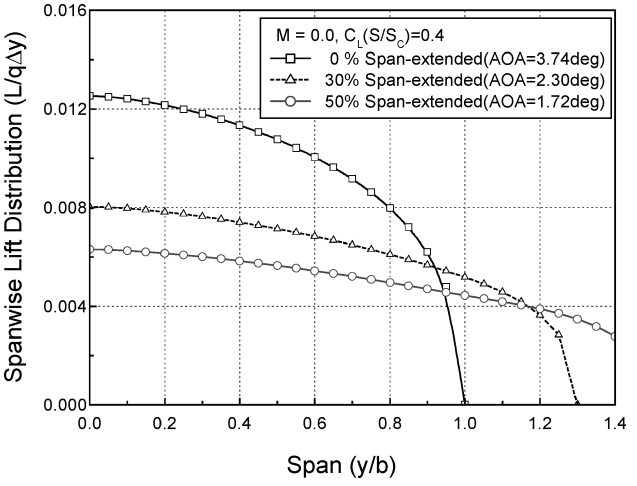


**Fig. 11 Spanwise lift distributions.**

increases as Mach number increases. When Mach number is 0.7, the lift coefficient of the 50% extended wing is 1.6 times of that of the original wing. Figure 9 shows the effect of the wing span on the lift coefficient when the AOA is 1.0 deg. Figure 9 shows that the lift coefficient of the morphing wing increases linearly as the wing span increases, and the lift coefficient derivatives increases as Mach number increases. Figure 10 shows the lift coefficient derivatives, as, obtained from a linear regression analysis of the data from Fig. 9, of the morphing wing as a function of wing span. The lift coefficient derivative is defined as

$$C_{Lye} = \frac{\partial C_L \bar{S}}{\partial (y_e/b)} \tag{13}$$

The derivatives increase exponentially as Mach number increases.

### Wing Load Distributions

Figure 11 shows the lift distribution along the span of the wing for a Mach number of 0.0 and a lift coefficient of 0.4. For this flight

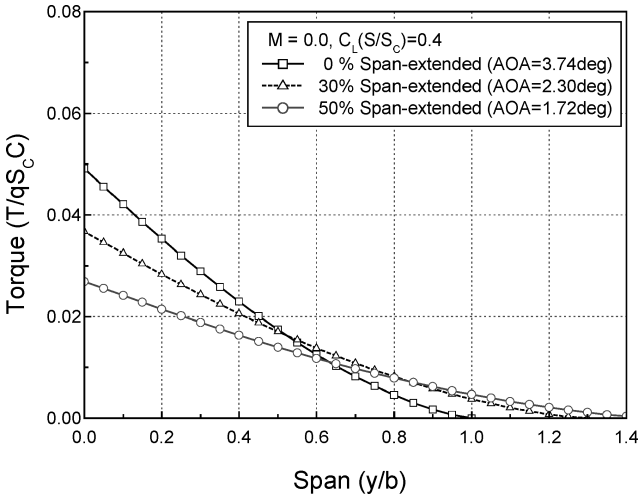


**Fig. 12 Torque distributions.**

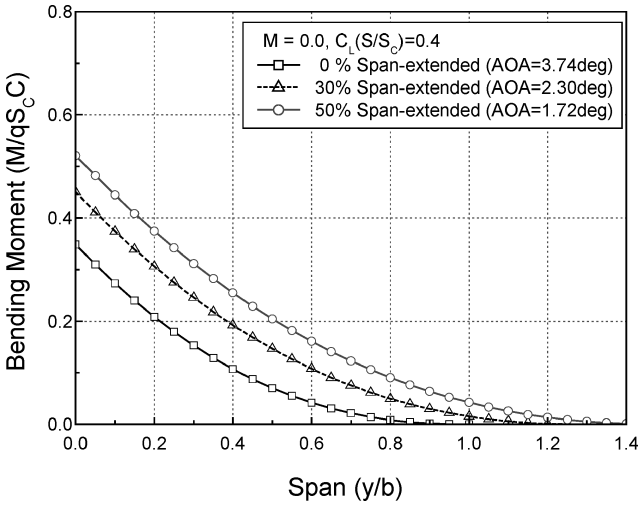


**Fig. 13 Bending moment distributions.**

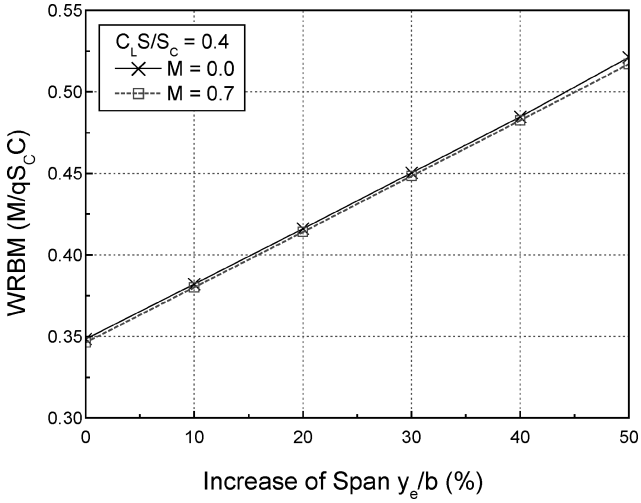


**Fig. 14 WRBM, $C_L\bar{S} = 0.4$.**

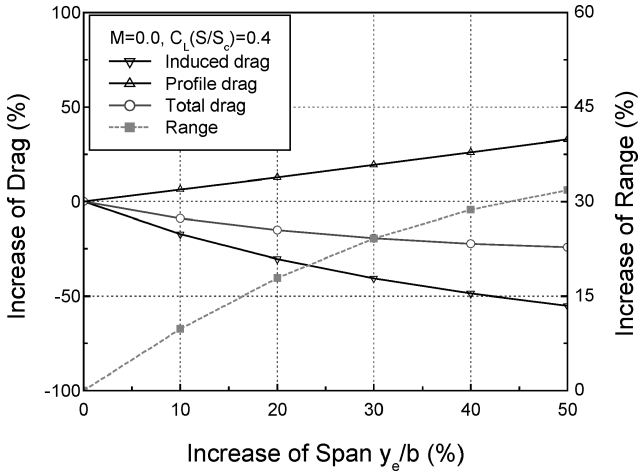


**Fig. 15 Effect of wing span on drag and range, $M = 0.0$ and $C_L\bar{S} = 0.4$.**

condition, the AOA of the morphing wing are 3.74, 2.30, and 1.72 deg for the 0, 30, and 50% span-extended cases, respectively. The area under the lift distribution is equal to the total lift produced by the morphing wing. To obtain the same lift, the lift per unit span decreases as the wing span increases. This means that the wing load of the VSMW is reduced as the wing span increases. Figure 12 shows the torque distribution along the wing span. Note that the elastic axis exists at 50% chord. The torque at the wing root decreases considerably as the wing span increases, whereas the torque at the wing tip increases only slightly. This means that the VSMW does not require larger wing torsional stiffness as compared with the conventional wing and the wing twist can be neglected in the design of the morphing wing. Figure 13 shows the bending moment distributions. In contrast to the torque distributions, the bending moment of the morphing wing increases considerably as its wing span increases. Here, the contribution of the moving wing on the bending moment significantly increases, although the spanwise lift decreases. Thus, the bending moment along the wingspan of the morphing wing is much larger than that of the conventional wing. Figure 14 shows the WRBM for the same flight condition ($C_L\bar{S} = 0.4$). The WRBM of the morphing wing increases linearly as the wing span increases. The WRBM for $M = 0.7$ is less than that for $M = 0.0$, but the difference is virtually nonexistent. The WRBM of the 50% span-extended morphing wing is increased by approximately 50% compared to that of the conventional wing. Therefore, we can assume that the wing deformation of the morphing wing due to the bending moment is more significant than that due to torque.

**Drag and Range**

The total drag of the aircraft wing is a combination of the induced drag and the profile drag. The profile drag can be approximated based on an empirical database and can be defined as

$$C_{D0} = a_0 + a_1 C_L + a_2 C_L^2 \tag{14}$$

where $a_0$, $a_1$, and $a_2$ are constants that are obtained by curve fitting the profile drag. Thus, total drag coefficient can be defined as

$$C_D = C_{D0} + C_{Di} \tag{15}$$

Figure 15 shows the changes in both drag and range of the morphing wing due to increased wing span. As the wing span increases, the induced drag decreases, whereas the profile drag increases linearly. The increase of the profile drag is due to the increase of the wing area, although the spanwise lift distributions decrease as shown in Fig. 11. The increase of the range can be calculated using[10]

$$R = 2\sqrt{2/\rho}(1/c_t)\left[(C_L S)^{\frac{1}{2}} / C_D S\right]\left(W_0^{\frac{1}{2}} - W_1^{\frac{1}{2}}\right) \tag{16}$$

where $c_t$, $W_0$, and $W_1$ are fuel consumption rate, gross weight with full tank, and gross weight with empty tank, respectively. The total drag of the morphing wing is decreased by approximately 25%, and its range is increased by approximately 30%. This range increase is the important advantage of the VSMW.

## Aeroelastic Characteristics

### Static and Dynamic Characteristics

Table 2 shows the static deformations of the morphing wing when the pressure acts on the upper skin. The total force due to pressure is 5.34 kN. For the 0% span-extended wing, the pressure is 17.2 kPa. For 30 and 50%, the pressures are 14.2 and 12.8 kPa, respectively. Although the same total force acts on theses wings, the wing-tip deformation of the 50% span-extended wing is larger than those of other wings. This means that the VSMW requires larger bending stiffness than the conventional wing.

Figure 16 shows the variations in natural frequency as the wing span increases. The natural frequency of the morphing wing decreases due to the increase in wing span. Because of to the 50% wing extension, the natural frequencies of the lowest four modes are considerably decreased by 36, 29, 50, and 34%, respectively. Thus, the structure of the VSMW becomes more flexible than the conventional wing.

### Aerodynamic Deformations and Divergence Speeds

The flight condition used for calculating the aerodynamic deformations of the VSMW is a Mach number of 0.0 and a lift coefficient $C_L\bar{S}$ of 0.4. When the modal matrix $[\phi]$ obtained from the free-vibration analysis and DHM code is used, the AICs $[\bar{Q}]$ in Eq. (9) are calculated and the second term $\{f_0\}$ in Eq. (9) is calculated for each AOA. The AOA for the 0, 30, and 50% span-extended morphing wings are 3.74, 2.30, and 1.72 deg, respectively.

Figures 17–19 show the deformed wing shapes of the 0, 30, and 50% span-extended wing when the Mach number is 0.0 and the lift coefficient is 0.4. When $[\bar{Q}]$ and $\{f_0\}$ are used, the aerodynamic deformations of the VSMW are calculated. When the dynamic pressure is 17 kPa, the maximum deformations at the wing tip of the main wing are 36.5, 97.9, and 213 mm for the 0, 30, and 50% span-extended wings, respectively, and the twist angles at wing tip are 1.7, 2.4, and 4.8 deg. The aerodynamic deformation increases as the wing span increases, and this is mainly due to the increase of the bending moment as shown in Figs. 13 and 14 rather than the torque in Fig. 12. Figure 20 shows the aerodynamic deformations of the morphing wing at the wing tip trailing edge (TE) and leading edge (LE). The aerodynamic deformations of the 50% span-extended wing increase dramatically. The wing tip deformations of the 0, 30, and 50% span-extended wing are greater than 10% of their wing spans when the dynamic pressures are 40, 20, and 15 kPa, respectively.

Figure 21 shows the divergence characteristics of the wing. When $[\bar{Q}]$ is used, the divergence dynamic pressure is calculated from Eq. (10). When Eq. 12 is used, the divergence speed can be calculated from the divergence dynamic pressure for a given flight altitude. Divergence is a statically unstable phenomenon. The divergence dynamic pressure of the 50% span-extended wing is 30 kPa when the Mach number is 0.0. But, the dynamic pressure of 20 kPa is defined as statically unstable because the aerodynamic

**Table 2 Applied pressures and static deformations of morphing wing**

| Wing span, % | Pressure, kPa | Wing-tip deflection, mm % |
|---|---|---|
| 0 | 17.2 | 64.6 (6.4 ) |
| 30 | 14.2 | 143 (11) |
| 50 | 12.8 | 230 (15) |

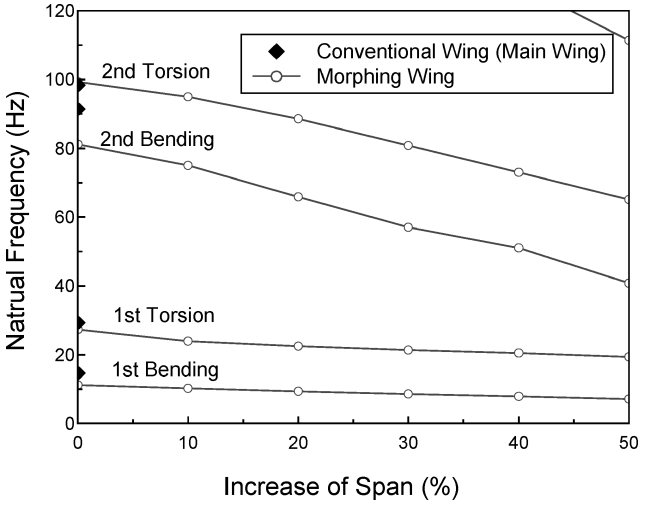


**Fig. 16 Variations of natural frequencies.**

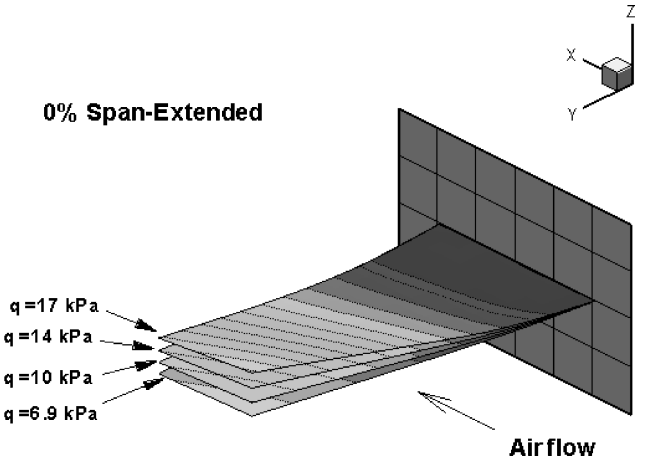


**Fig. 17 Aerodynamic deformations of 0% span-extended morphing wing, $C_L\bar{S} = 0.4$.**

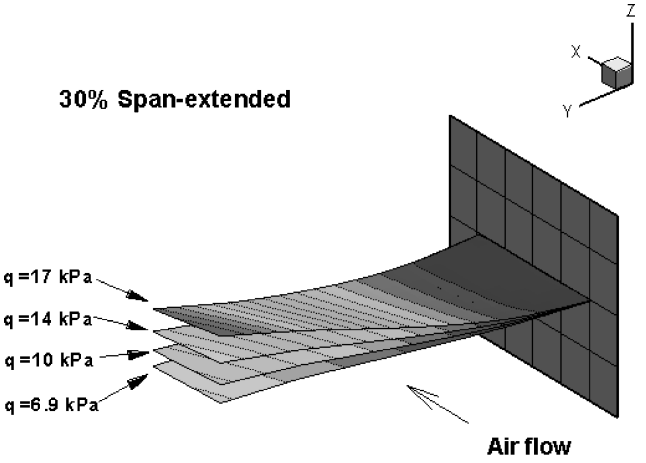


**Fig. 18 Aerodynamic deformations of 30% span-extended morphing wing, $C_L\bar{S} = 0.4$.**

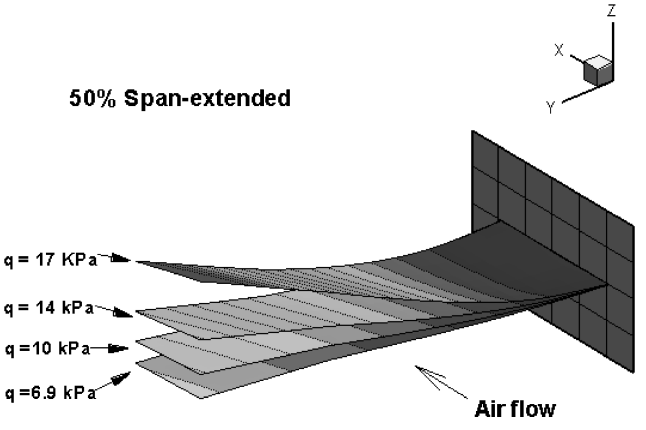


**Fig. 19 Aerodynamic deformations of 50% span-extended morphing wing, $C_L\bar{S} = 0.4$.**

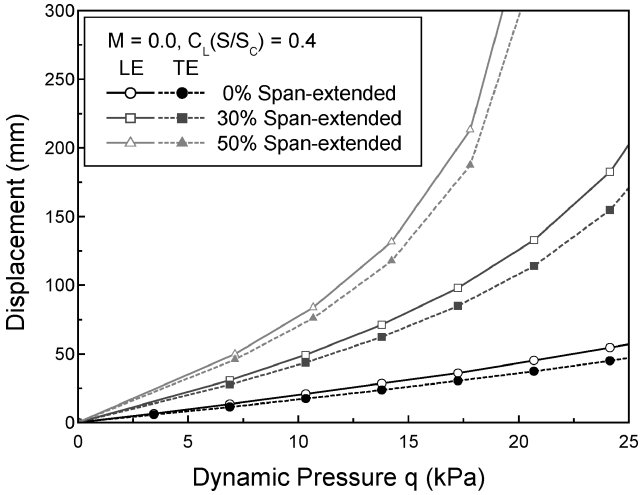


**Fig. 20 Aerodynamic deformation at wing tip of main wing, $C_L\bar{S} = 0.4$.**

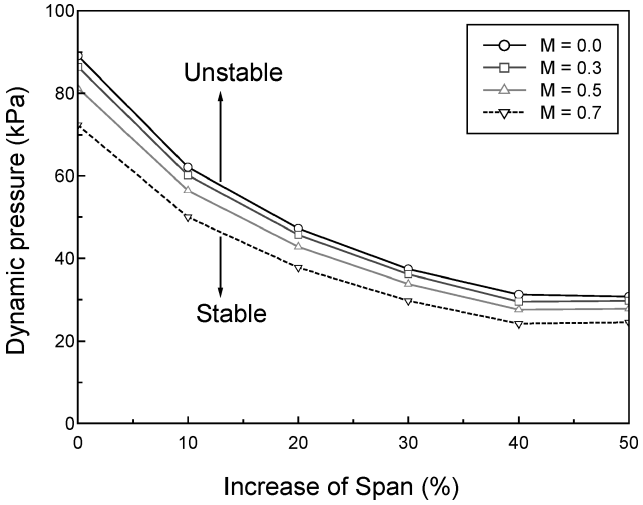


**Fig. 21 Divergence characteristics of VSMW.**

deformation is too large: The wing-tip displacement is larger than 10% of the wing span. The divergence boundary considerably decreases as the wing span increases. Hence, the aeroelastic characteristics of the VSMW become worse, and it is important to investigate static aeroelastic stability.

## Conclusions

In this study, a VSMW is considered for reducing induced drag and increasing the range of a long-range cruise missile. Both, static aerodynamic and aeroelastic characteristics of the wing are investigated. From the aerodynamic analysis, the effects of increasing the wing span and the Mach number are studied. The results indicate that, due to the increased wing span, the spanwise lift distributions and the induced drag are considerably decreased; however, the WRBMs are considerably increased.

The aeroelastic analysis shows that the flexibility of the morphing wing structure increases as the wing span increases. At a given flight condition, the aerodynamic deformation is much larger than that of the conventional wing. Static aeroelastic considerations show that a VSMW requires increased bending stiffness because the wing deformation due to bending is much more significant than the deformation due to twist, which demands that VSMW designers include larger bending stiffness in their formulation.

Finally, we show that the important advantages of a VSMW are a drag reduction and an increase of range. However, the increase of the wing span can cause large deformations. Therefore, the designer should consider aeroelastic phenomenon in the design of a VSMW.

## Acknowledgments

This work was supported by the Postdoctoral Fellowship Program of the Korea Science and Engineering Foundation and, in part, by the Defense Advanced Research Projects Agency's Morphing Aircraft Structures Program under the direction of Terrence A. Weisshaar. The support is gratefully acknowledged. Also, authors express thanks to the associate editor and reviewers for many valuable comments and suggestions.

## References

[1]Bowman, J., Sanders, B., and Weisshaar, T., "Evaluating the Impact of Morphing Technologies on Aircraft Performance," AIAA Paper 2002–1631, April 2002.

[2]Gern, F. H., Inman, D. J., and Kapania, R. K., "Structural and Aeroelastic Modeling of General Planform Wings with Morphing Airfoils," *AIAA Journal*, Vol. 40, No. 4, 2002, pp. 628–637.

[3]Sanders, B., Eastep, F. E., and Foster, E., "Aerodynamic and Aeroelastic Characteristics of Wings with Conformal Control Surfaces for Morphing Aircraft," *Journal of Aircraft*, Vol. 40, No. 1, 2003, pp. 94–99.

[4]Amprikidis, M., and Cooper, J. E., "Development of Smart Spars for Active Aeroelastic Structures," AIAA Paper 2003–1799, April 2003.

[5]Blondeau, J., Richeson, J., and Pines, D. J., "Design, Development and Testing of a Morphing Aspect Ratio Wing Using an Inflatable Telescopic Spar," AIAA Paper 2003–1718, April 2003.

[6]Bae, J. S., Yang, S. M., and Lee, I., "Linear and Nonlinear Aeroelastic Analysis of a Fighter-Type Wing with Control Surface," *Journal of Aircraft*, Vol. 39, No. 4, 2002, pp. 697–708.

[7]Ueda, T., and Dowell, E. H., "A New Solution Method for Lifting Surfaces in Subsonic Flow," *AIAA Journal*, Vol. 20, No. 3, 1982, pp. 348–355.

[8]Eversman, W., and Pitt, D. M., "Hybrid Doublet Lattice/Doublet Point Method for Lifting Surfaces in Subsonic Flow," *Journal of Aircraft*, Vol. 28, No. 9, 1991, pp. 572–578.

[9]Striz, A. G., and Venkayya, V. B., "Influence of Structural and Aerodynamic Modeling on Flutter Analysis," *Journal of Aircraft*, Vol. 31, No. 5, 1994, pp. 1205–1211.

[10]Anderson, J. D., Jr., *Introduction to Flight*, McGraw–Hill, New York, 1985, pp. 298–303.